Achieving highly-efficient H_2S gas sensor by flower-like SnO_2–SnO/porous GaN heterojunction

Zeng Liu(刘增)[1,2,†], Ling Du(都灵)[3], Shao-Hui Zhang(张少辉)[4,‡], Ang Bian(边昂)[5], Jun-Peng Fang(方君鹏)[6], Chen-Yang Xing(邢晨阳)[7], Shan Li(李山)[8], Jin-Cheng Tang(汤谨诚)[8], Yu-Feng Guo(郭宇锋)[1,2], and Wei-Hua Tang(唐为华)[1,2,§]

[1] *College of Integrated Circuit Science and Engineering, Nanjing University of Posts and Telecommunications, Nanjing* 210023, *China*
[2] *National and Local Joint Engineering Laboratory for RF Integration and Micro-Packing Technologies, Nanjing University of Posts and Telecommunications, Nanjing* 210023, *China*
[3] *School of Electronic and Information Engineering, Jinling Institute of Technology, Nanjing* 211169, *China*
[4] *Institute of Microscale Optoelectronics, Shenzhen University, Shenzhen* 518060, *China*
[5] *Key Laboratory of Luminescence and Optical Information of Ministry of Education, Institute of Optoelectronic Technology, Beijing Jiaotong University, Beijing* 100044, *China*
[6] *School of Integrated Circuits, Tsinghua University, Beijing* 100084, *China*
[7] *Key Laboratory of Optoelectronic Devices and Systems of Ministry of Education, College of Physics and Optoelectronic Engineering, Shenzhen University, Shenzhen* 518060, *China*
[8] *State Key Laboratory of Information Photonics and Optical Communications, School of Science, Beijing University of Posts and Telecommunications, Beijing* 100876, *China*

(Received 4 February 2022; revised manuscript received 19 April 2022; accepted manuscript online 22 April 2022)

A flower-like SnO_2–SnO/porous GaN (FSS/PGaN) heterojunction was fabricated for the first time via a facile spraying process, and the whole process also involved hydrothermal preparation of FSS and electrochemical wet etching of GaN, and SnO_2–SnO composites with p–n junctions were loaded onto PGaN surface directly applied to H_2S sensor. Meanwhile, the excellent transport capability of heterojunction between FSS and PGaN facilitates electron transfer, that is, a response time as short as 65 s and a release time up to 27 s can be achieved merely at 150 °C under 50 ppm H_2S concentration, which has laid a reasonable theoretical and experimental foundation for the subsequent PGaN-based heterojunction gas sensor. The lowering working temperature and high sensitivity (23.5 at 200 ppm H_2S) are attributed to the structure of PGaN itself and the heterojunction between SnO_2–SnO and PGaN. In addition, the as-obtained sensor showed ultra-high test stability. The simple design strategy of FSS/PGaN-based H_2S sensor highlights its potential in various applications.

Keywords: gas sensor, SnO_2–SnO, porous GaN, heterojunction

PACS: 07.07.Df **DOI:** 10.1088/1674-1056/ac6947

1. Introduction

H_2S usually refers to extremely harmful manure and sewer gas in human daily life.[1] At low concentrations close to 5 ppm, it smells like rotten eggs. At a high concentration of more than 50 ppm, it will irritate the eyes and the respiratory system. The sense of odors disappears as the olfactory nerves have been paralyzed when the gas concentration reaches above 100 ppm. Therefore, efficient gas sensors with a fast response with regard to the high-sensitivity detection of H_2S in the surrounding environment are urgently required.

Nowadays, gas sensors play a vital role in most domains of intelligent sensing technology. Among all kinds of gas sensors, semiconductor metal oxides (MOs)[2–6] sensors (such as SnO_2, ZnO, and WO_3) have always been the spotlight due to their low cost, out-bound sensitivity, low power consumption and easiness of fabrication. By and large, the MOs sensors are divided into n-type MOs[7,8] and p-type MOs.[9,10] Generally, n-type MOs are more advantageous for use as gas sensors than p-type MOs such as higher carrier mobilities. As a typical n-type semiconductor, the application of SnO_2 ($E_g = 3.6$ eV) gas sensor has been investigated for a long time. Despite the advantages of SnO_2 over other materials, such as higher sensitivity and faster response time, practical applications of SnO_2 are still subject to the limitations of temperature and water vapor poisoning,[11,12] even poor selectivity.[13] These constraints have severely affected the further promotion of SnO_2-based gas sensors. Thereafter, it is found that SnO_2/p-type metal oxides hybrid sensing materials can effectively overcome some shortcomings.[14–17]

Traditional MOs sensors are composed of the sensitive layer depositing on substrate Al_2O_3 or Si,[18,19] and a miniature heater is usually installed on the back of substrate. Compared with Al_2O_3 just only as support substrate, Si has been confirmed to be responsive to several gases.[20–22] With changes in the working environment of gas sensors (includ-

†Corresponding author. E-mail: zengliu@njupt.edu.cn
‡Corresponding author. E-mail: shzhang2016@sinano.ac.cn
§Corresponding author. E-mail: whtang@njupt.edu.cn

© 2023 Chinese Physical Society and IOP Publishing Ltd

ing high pressure, strong corrosion, etc.) and the future development trend of multi-sensor integration,[23–25] GaN shows higher stability and superiority. GaN, known as a wide direct bandgap (3.39 eV) material, has a superior thermal conductivity, a large saturation electron drift velocity and excellent thermostability apart from good acid and alkali resistance. Accordingly, GaN based MO gas sensors has been noticed. Especially, since 2016, Pan's team[26–28] proposed a variety of GaN nanostructures with different shapes, sizes, and depths through electrochemistry, photoelectrochemistry, direct photochemistry, and metal-assisted photochemistry etching methods, which had been successfully applied to various biochemical sensors, constructed surface-enhanced raman scattering (SERS) substrates, and photoluminescence, and porous GaN (PGaN) was especially noticeable among them. On the one hand, the PGaN is not only more stable than porous Si, but also has response to certain gases.[29,30] On the other hand, the porous structure itself is more propitious for the gas flow and offers larger specific surface (beneficial to the sensitive material attached).[31] In previous work,[32] we reported a heterojunction of ZnO/PGaN and directly applied to a diode-type humidity sensor, except for the high response value, the response and release time within a wide range of relative humidity (RH) levels have also been enhanced.

In order to develop practically useful H_2S sensors, herein, SnO_2–SnO/PGaN heterojunction sensor was fabricated by a facile spraying method, and involving hydrothermal preparation of flower-like SnO_2–SnO and electrochemical wet etching of GaN throughout the assembly process. The prepared SnO_2–SnO composites with PGaN substrate could effectively enhance the gas response to the H_2S and reduce the working temperature. A highly plausible charge transport mechanism based on physical and chemical adsorbed H_2S layers was raised to elucidate the tested gas sensing response at lowering temperature.

2. Experimental details

2.1. Chemicals

Anhydrous ethanol (C_2H_5OH), acetone (C_3H_6O), sulfuric acid (H_2SO_4, 98%), urea (H_2NCONH_2) and $SnCl_4{\cdot}2H_2O$ were supplied by Sinopharm Chemical Reagents Co., Ltd, GaN pitaxial wafers were purchased from Suzhou Nanowin Science and Technology Co., Ltd, and ionic liquid (ILs) [EMIM][OTF] was purchased from Shanghai Chengjie Chemical Co., Ltd.

2.2. Materials preparation

2.2.1. PGaN preparation

Single-crystal n-type GaN (0001) films were grown on sapphires (0001) by hydride vapor phase epitaxy (HVPE). The size of GaN slice is 1.0 cm ×0.3 cm and the Si-doped GaN layer is 5 μm thick. The PGaN substrate was prepared by a photo-assisted electrochemical etching (Fig. 1(a)). Before etching, the GaN sample was sequentially ultrasonic cleaned by acetone, absolute ethanol and deionized (DI) water, then the surface was dried with high-purity N_2, also performed UV/O_3 vacuum plasma treatment to enhance the hydrophilicity and improve the binding capacity between the etching solution and GaN through surface modification, as shown in Fig. 1(b). The silver lead and GaN were connected by a conductive silver paste to form an ohmic contact. Meanwhile, the GaN sample and Pt plate were put into [EMIM][OTF] as the anode and cathode in the illumination with a 300 W xenon lamp. The etching voltage was 5 V and the etching time was 20 min. After etching, PGaN was immersed in 1 M oxalic acid solution for 3 h to clean the surface and then rinsed with deionized water.

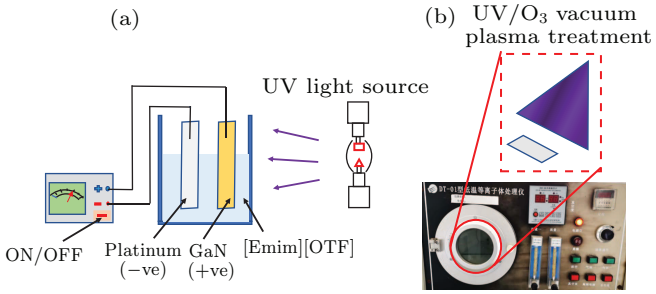


Fig. 1. Schematic diagram of (a) the photo-assisted electrochemical etching GaN and (b) the GaN epitaxial wafer was pre-treated using UV/O_3 vacuum plasma treatment.

2.2.2. SnO_2–SnO composites preparation

We synthesized the SnO_2–SnO complexes by one-step hydrothermal method. In typical synthetics, 0.108 g of urea and 0.132 g of $SnCl_4{\cdot}2H_2O$ were dissolved into 30 mL of DI water under modest stirring for around 30 min until a homogeneous emulsion formed. Then, the mixed solution was transferred to 50 mL hydrothermal reactors in which the hydrothermal reaction was performed at 180 °C for 18 h. Next, the SnO_2–SnO composites could be formed by washing with DI water and anhydrous ethanol by centrifuging at 2500 rpm, and finally dried at 70 °C for 2 days in air.

2.3. Fabrication of the heterojunction

The etched PGaN was fixed on a heating platform at a controlled temperature of 90 °C, and the SnO_2–SnO/ethanol dispersion was sprayed onto the PGaN surface by using the spraying gun to maintain a relatively constant moving speed and distance. Obviously, it was essential to maintain the balance between the spraying gun pressure/the moving speed and the distance. Then the Ag electrode was placed on the surface of the PGaN as the bottom electrode, and the Ag electrode at the other end was placed on the SnO_2–SnO layer as the top

electrode to construct the FSS/PGaN heterojunction. As a contrast, the SnO_2–SnO layer was sprayed on Al_2O_3 in the same manner.

2.4. Gas sensing measurements

The as-obtained gas sensor was placed in an inert, airtight telflons chamber in which H_2S, NO_2 and H_2 were carried by zero grade dry air. The specific testing equipment and the whole testing process could be learned about from the previous work.[33]

3. Results and discussion

3.1. Preparation and characterization of the PGaN substrate and the SnO_2–SnO sensing materials

In this study, the PGaN substrate was prepared by a photo-assisted electrochemical etching. In the photo-assisted electrochemical etching process,[28] two-thirds of the GaN epitaxial wafer were immersed in the [EMIM][OTF] under the influence of light and electric energy. The electrons were excited from the valence band to the conduction band, thereby forming holes in the valence band.[34] As the reaction proceeded, the holes were internally transferred to the interface between GaN and the ILs, and interacted with the active anion at the interface. The triple bond between the Ga atom and the N atom was broken, and Ga formed a compound with the anion in the form of Ga^{3+}. N atoms were combined with each other to generate N_2. The reactions from the GaN and the ILs could be described as follows:

$$2GaN + 6h^+ + 6CF_3SO_3 = 2Ga(CF_3SO_3)_3 + N_2\uparrow.$$

The SEM images of PGaN were shown in Fig. 2(a), and the PGaN possessed an orderly and uniform pores distribution with average size about 50 nm. The inset in Fig. 2(a) showed the etching depth was about 830 nm, and the calculated average etching rate is 41.5 nm/min. The FSS gas sensing materials were prepared via one-step hydrothermal method. During the hydrothermal reaction process, H_2NCONH_2 played a critical role during the emergence of the SnO_2–SnO complexes, which hydrolyzed to form NH^{4+} and CO_3^{2-} when the temperature was higher than 90 °C. With further increase in temperature, H_2NCONH_2 produced CO_3^{2-} and OH, respectively. Due to the limited amount of oxygen in the solution and the air of teflon-lined vessel, only a bit amount portion of SnO could be turned into SnO_2 to bring into being SnO_2–SnO composites. The main reactions from the Sn^{2+} and Sn^{4+} could be described in supporting information (Fig. S1). Figures 2(b) and 2(c) showed SEM images of the SnO_2–SnO hybrids at different scales. It could be seen that the sample presented an uneven spheroidal structure, consisting of nanosheets and nanoparticles. The sample displayed a 3D flower-like structure between 100–200 nm, assembled from nanosheets about 8–10 nm in thickness. The high-resolution TEM (HRTEM) showed the detailed microstructural and crystallographic properties of the as-prepared SnO_2–SnO composites. Figures 2(d) and 2(e) exhibited the layered structure of the nanosheets sample. The HRTEM image in Fig. 2(f) revealed the well-defined lattice fringes with the interplanar spacings of 0.27 nm, 0.24 nm and 0.33 nm, corresponding to the (110) and (002) lattice planes of SnO and (110) lattice plane of SnO_2, respectively.

The components and crystal structures of the as-prepared sample were characterized by x-ray diffraction analysis techniques (XRD) and scanning electron microscopy (including of EDS and XPS). Figure 3(a) exhibited the XRD pattern of

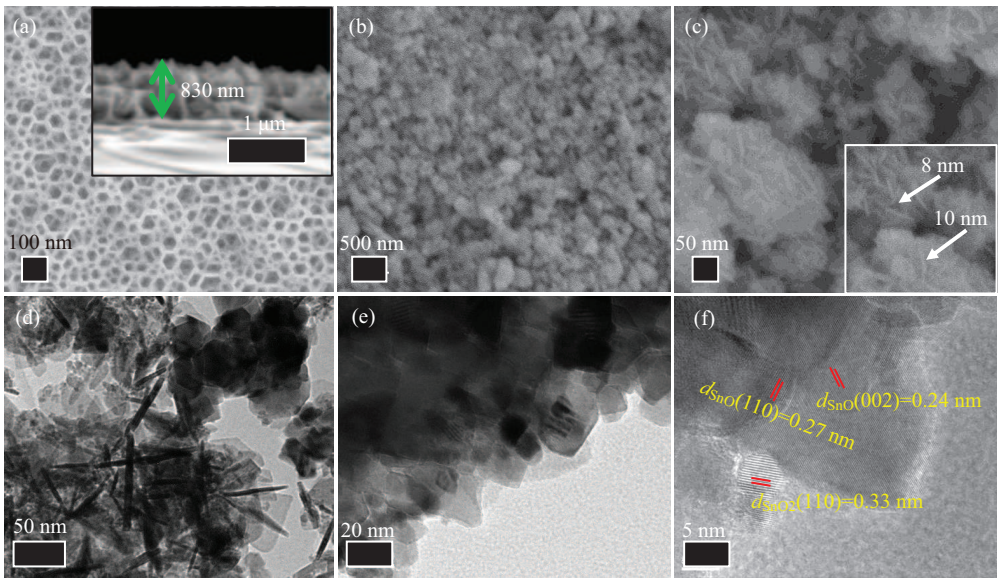


Fig. 2. (a) SEM images of the PGaN. Inset: cross-sectional SEM of etched PGaN. (b), (c) SEM images of the SnO_2–SnO composites at different scales. Inset: partially enlarged flower-like SnO_2–SnO. (d), (e) TEM images of the SnO_2–SnO composites at different scales. (f) HRTEM images of the SnO_2–SnO composites.

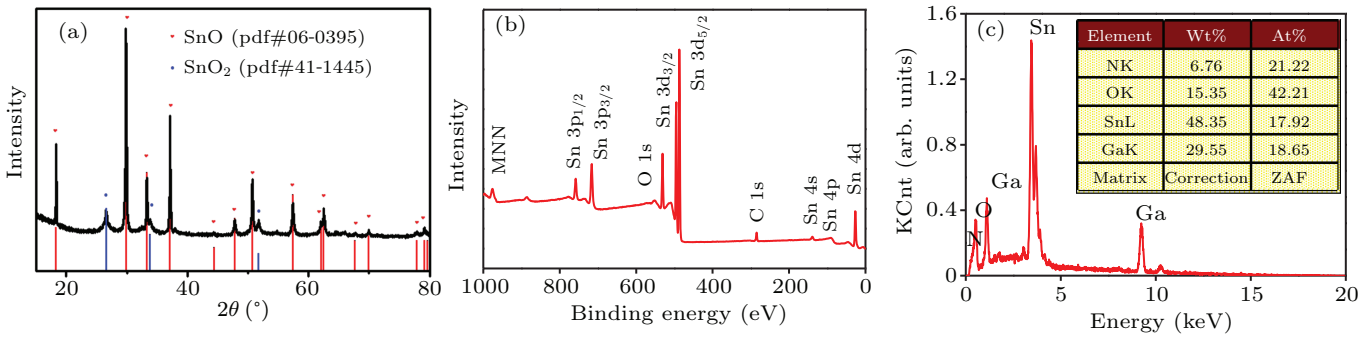


Fig. 3. (a) XRD patterns of the SnO_2–SnO composites. (b) Full XPS spectrum of the SnO_2–SnO composites. (c) EDS elemental analysis for SnO_2–SnO/GaN heterojunction.

the heterojunction-structured SnO_2–SnO composites, showing the peaks were consistent with of that of standard cassiterite (SnO_2) and romarchite (SnO). In the XRD pattern of SnO_2–SnO, the intensity and full width at half maxima (FWHM) of the diffraction peaks from the SnO_2 were much weaker and wider than those from the SnO component, indicating that the SnO_2 nanocrystals were much smaller than the SnO nanoparticles.

XPS measurements were performed to determine the chemical states of the SnO_2–SnO complexes. Figure 3(b) showed the XPS in the range of 0–1000 eV binding energy. Visibly, there were no other impurities peaks observed except for Sn, O and C. The specific spectrum of Sn and O could be exhibited in Fig. S1. The XPS results were consistent with the XRD measured pattern results. Above XPS and XRD characterization both indicated that the SnO_2–SnO complexes has been successfully prepared through the facile one-step hydrothermal reaction process. Figure 3(c) displayed that the EDS elemental analysis confirmed the existence of Sn, O, Ga and N elements from the FSS/PGaN heterojunction. In total, XRD and XPS measurements were consistent with these electron microscopy results, indicating that the p–n heterostructure of SnO_2–SnO was formed by large SnO layered crystals surrounded by small SnO_2 nanoparticles.

For further confirming the structure of SnO_2–SnO/PGaN, nitrogen adsorption and desorption measurements and BJH pore size distribution analysis were performed. As shown in Fig. S2, the specific surface area and pore size construction of SnO_2–SnO and SnO_2–SnO/PGaN were comparably evaluated. The specific surface areas of SnO_2–SnO and SnO_2–SnO/PGaN were 158.31 $m^2 \cdot g^{-1}$ and 218.29 $m^2 \cdot g^{-1}$, respectively. This result displayed that the composite had a larger surface area and stronger gas adsorption than PGaN. While SnO_2–SnO/PGaN displayed a type IV isotherm with a H3 hysteresis loop in Fig. S2(a), the SnO_2–SnO/PGaN composite also exhibited dual desorption characteristics of SnO_2–SnO and PGaN, which indicated that the composite possessed pore structures of SnO_2–SnO and PGaN. The SnO_2–SnO/PGaN composite possessed the hierarchical pores consisting of micropores and mesoporous from the PGaN and tightly packing of SnO_2–SnO nano-flowers (Fig. S2(b)). In addition, the SnO_2–SnO/PGaN composite also contained some additional mesopores and macropores that came from the interspaces between SnO_2–SnO and PGaN. The above pores of SnO_2–SnO/PGaN acted as direct channels of diffusion for target gas molecules and promoted rapid adsorption/desorption of gas molecules at the interface. All results demonstrated that the SnO_2–SnO grew on the PGaN surface and formed the composite, which was an ideal composite for enhancing gas performances.

3.2. H_2S sensing performance test of the SnO_2–SnO/PGaN

The working temperature is one of the significant sensing properties of sensitive materials. Figure 4(a) demonstrated the response curves of the SnO_2–SnO/PGaN and SnO_2–SnO/Al_2O_3 at 50 ppm, 100 ppm and 200 ppm H_2S as a function of working temperature. As could be seen, the response value (sensitivity S) was closely related to the working temperature. The sensitivity first reached a peak and then decreased as the temperature increased further. Also, the sensitivity also increased as the concentration of H_2S increases, which showed sets of sensitivity of 6.3, 12.2 and 23.5 at 50 ppm, 100 ppm and 200 ppm, respectively.

The sensitivity in this work is defined as

$$S = R_a/R_g,$$

where R_a and R_g are the resistances in air and H_2S gas, respectively.

Apparently, it was closely related to the presence of PGaN substrates. Specifically, heterojunction generated between the SnO_2–SnO and PGaN, the high electron mobility of the porous GaN itself both accelerated the electron transfer rate, which were the main drivers for lowering the sensor operating temperature. The dynamic sensing response and release properties of the SnO_2–SnO/PGaN for H_2S detection were investigated. Figures 4(b) and 4(c) displayed the sensing responses of the SnO_2–SnO/PGaN as a function of the concentration of H_2S (from 10 ppm to 50 ppm and from 80 ppm to 200 ppm) at 150 °C, indicating response effect with steadily increas-

ing sensitivity. Meanwhile, the linear relationship of sensitivity with H_2S concentration (from 10 ppm to 200 ppm) was also confirmed in Fig. 4(d). In addition, the resistance of the sensor was fully restored when it was exposed to fresh air throughout the test. The response and release times are 47 s and 37 s, respectively (Fig. 4(e)). The sensing selectivity of the SnO_2–SnO/PGaN for H_2S was also studied. As shown in Fig. 4(f) with the SnO_2–SnO/PGaN sensor exposed to 50 ppm H_2S, NO_2, H_2 and C_2H_5OH at 150 °C, the response (S) to H_2S was distinctly far greater than those to NO_2, H_2 and C_2H_5OH gases, demonstrating the clearly distinguishable selectivity of the dual heterojunction (SnO_2–SnO p–n and SnO_2–SnO/PGaN heterojunction) nanostructure for H_2S detection.

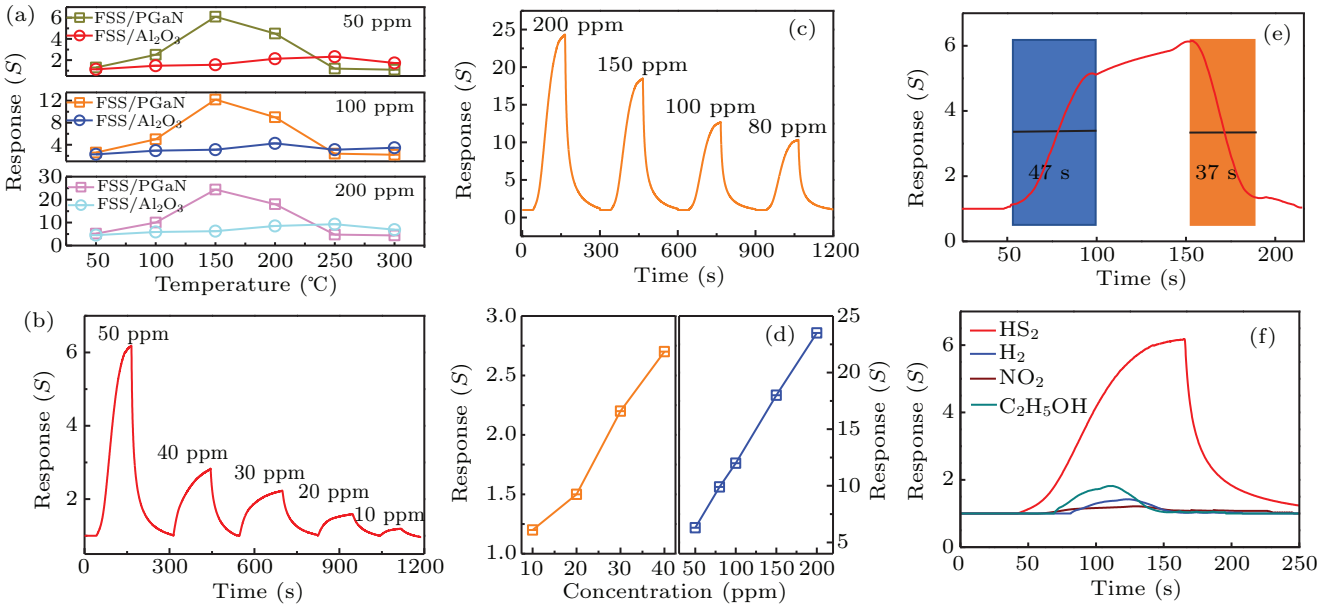


Fig. 4. (a) Sensing response curves of FSS/PGaN and pure SnO_2–SnO to 50 ppm H_2S as a function of the working temperature at different H_2S concentrations. Sensing response curves of SnO_2–SnO/PGaN exposure to H_2S with different concentrations varying from (b) 10 ppm to 50 ppm and (c) 80 ppm to 200 ppm. (d) Variation curves of response (S) with different gas concentrations. (e) One response/release cyclic curve of SnO_2–SnO/PGaN at 50 ppm H_2S. (f) Gas selectivity comparative curves of FSS/PGaN to 50 ppm H_2S, H_2, NO_2 and C_2H_5OH at 150 °C.

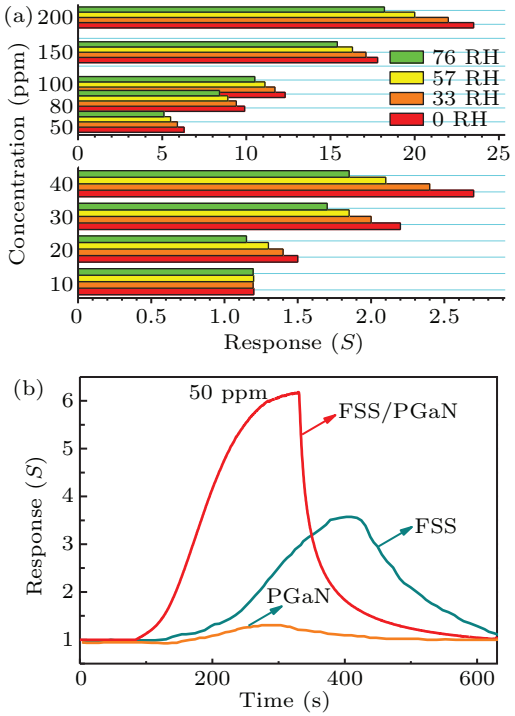


Fig. 5. (a) Histogram of the response value varied with H_2S concentration under different RH. (b) Response curves of sensors based on PGaN, FSS or FSS/PGaN at 50 ppm H_2S.

Relative humidity (RH) has a great influence on different types of gas sensors, and for this regard, we have compared the gas response performance under different humidity conditions, as shown in the Fig. 5(a). The results showed that the sensitivity of the sensor exhibited a decreasing trend with increasing RH, and the decreasing trend became more conspicuous with increasing H_2S concentration. Specifically, the sensitivities were 23.5, 22.0, 20.1 and 18.2 when the RH were 0%, 33%, 57% and 76% at 200 ppm, respectively. The effect of RH on sensitivity was mainly due to hopping and Grotthus transport mechanisms.[35] In addition, Fig. 5(b) presented the response curves at 50 ppm H_2S for the PGaN, FSS and FSS/PGaN-based sensors, where the pure PGaN-based sensor gave extremely weak response value for H_2S, much smaller than the FSS and FSS/PGaN-based sensors. However, the gas sensing materials of FSS and FSS/PGaN-based sensors were both flower-like SnO_2–SnO, their morphology and microstructure were similar, and the sensitivity and the response speed of FSS/PGaN were yet higher than FSS-based sensor. Therefore, the heterojunction effect between FSS and PGaN was highlighted, and the signal amplification function of the heterojunction made the property of FSS/PGaN-based sensor exceed a single FSS or PGaN-based devices.

The repeatability is an important factor for practical ap-

plication of gas sensor. Simultaneously, five reversible and similar cyclic peaks of the FSS/PGaN-based gas sensor toward 50 ppm H_2S was exhibited at 150 °C in Fig. 6(a), indicating superb response/release property. Long-term stability is another significant performance parameter of gas sensor in real application. Figure 6(b) illustrated a negligible fluctuation ratio $\sim 2.5\%$ relative to initial response value after more than 6 months continuous monitoring, demonstrating that as-prepared sensor was of prominent long-term stability and relatively reliable application prospects.

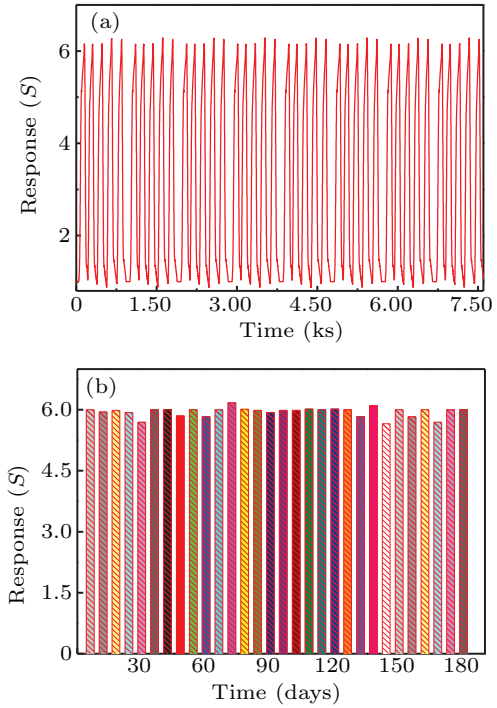


Fig. 6. (a) Response (S)–time curve of 5 response/release cyclic peaks. (b) Histogram of gas response values (S) recorded for half a year.

By considering the rare reports of pure SnO or SnO_2–SnO based H_2S gas sensor (mostly reported SnO_2–SnO based NO_2 or H_2 sensor), Table 1 demonstrated the comparison of the operating temperature and response/release time of the sensor in this work with SnO_2 and other MO based H_2S sensors reported. Thus, the construction of FSS/PGaN based H_2S sensor was a major breakthrough in this domain. The FSS/PGaN based H_2S sensor showed improved overall performance involving all parameters as opposed to other H_2S sensors. The response time was 65 s when the gas concentration changed from 0 ppm to 50 ppm, which was closely related to the time for H_2S gas to penetrate into the PGaN layer. The as-obtained sensor displayed potential for rapid gas sensing over a wide range of H_2S concentration variations. It is worth mentioning that the release time was 27 s when H_2S concentration was converted from 50 ppm to 0 ppm. The release time of H_2S gas sensor was faster than the response time, which was mostly dominated by the desorption time of H_2S gas from the FSS layer. Moreover, the release time of FSS/PGaN based H_2S gas sensor was still faster than that of some SnO_2 and other MO based H_2S gas sensors reported in the prior literature of others. Given that the FSS/PGaN based H_2S sensor had only two components, including of high sensitivity and the special PGaN substrate. In concrete terms, for one side, high sensitivity could be mainly ascribed to the enhanced dispersity of FSS. For other side, the characteristic of high electron mobility of PGaN could accelerate the electron transfer rate to make SnO_2–SnO quickly react with H_2S. Therefore, the FSS/PGaN heterojunction presented potential for fast H_2S sensing.

Table 1. Main performance parameters comparison of H_2S gas sensor.

Sensing material	Operating temperature (°C)	H_2S concentration (ppm)	Response/release time (s)	Interfering	Reference
CuO-NiO	260	100	18/29	NO_2/ethanol	[36]
TiO_2–Fe_2O_3	300	200	–	SO_2/CO	[37]
Co_3O_4–SnO_2	180	10	25/160	–	[38]
SnO_2NW/rGO	22	50	2/292	NH_3/SO_2/N_2/ethanol	[39]
ZnO/SnO_2	300	10	–	NO/SO_2/CO/CH_4	[40]
SnO_2 NF	350	1	15/230	NO/SO_2/CO/CH_4	[41]
SnO_2–SnO/GaN	150	200	65/27	H_2/NO_2/ethanol	this work

3.3. Gas sensing mechanism of the SnO_2–SnO/PGaN sensor with heterojunctions

In most gas sensing response systems, gas sensing mechanisms are generally analyzed in terms of adsorption/desorption model (including oxygen sorption models, chemical adsorption/desorption and physical adsorption/desorption), bulk resistance control mechanism and gas diffusion control mechanism.[42] In our experimental system, we focused on PGaN intrinsic property (gas diffusion control mechanism) and the adsorption–desorption model (mainly oxygen adsorption model and chemisorption-desorption dominated) of the p–n heterostructure formed by the MO.

From the above studies, the SnO_2–SnO/PGaN sensor exhibited improved sensing properties compared with the SnO_2–SnO/Al_2O_3 sensor. For gas diffusion control mechanism, this mechanism was more focused on the gas diffusion process, and the most important factor affecting this process was the morphology of the material. Gas diffusion in the whole process was a dynamic transition between the surface chemical

reaction (SCR) and the rate-determining step (RDS), and the condition depended on transition temperature stage, pore canal model[43] and hollow sphere model[44–46] gave a good account of the relationship between these two responses and their operating intervals. The gas diffusion control mechanism was limited by the quantitative analysis of multiple factors and needed to be optimized, but it did not affect the index used by the model to evaluate the effect of the MO-based gas sensor morphology on performance.

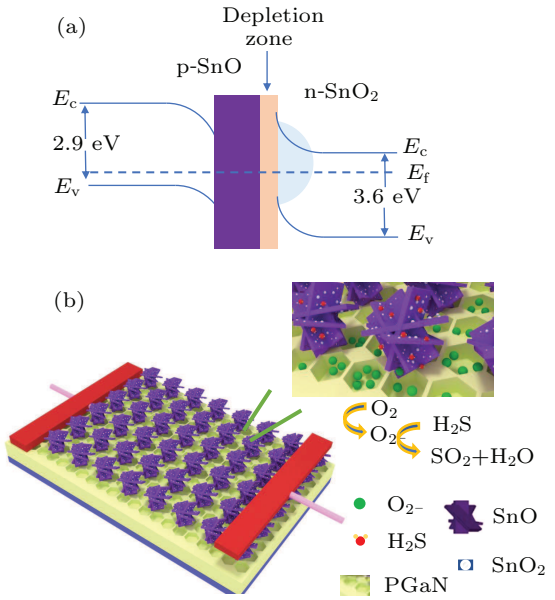


Fig. 7. (a) Schematic diagram of the heterostructure of the n-SnO_2 nanoparticles on the surface of the p-SnO nanosheets with a p–n junction. (b) H_2S sensing mechanism of SnO_2–SnO/PGaN heterojunction.

The sensing mechanism of the SnO_2–SnO/PGaN was meant to be heterojunction nanostructure for the adsorption-desorption model. The n-type SnO_2 and p-type SnO developed a heterojunction structure at the interface first, as illustrated in Fig. 7(a).[47,48] SnO_2 and SnO have forbidden band widths of 3.6 eV and 2.9 eV, respectively. The creation of a depletion area is caused by the p–n junction.[1] The schematic illustration of the SnO_2–SnO/PGaN sensor was shown in Fig. 7(b). SnO_2–SnO/PGaN gas sensitivity was recognized to be altered by the interaction between gas species and adsorbed oxygen. Upon energization, the electrons were excited from SnO_2–SnO composites and formed electron-hole pairs. Excited electrons could contribute to turning adsorbed oxygen to O^{2-} and O. The thickness of the electron depletion layer increased with large amounts of adsorbed oxygen surged, and thus affected the operating temperature. Because of chemisorption, H_2S molecules adsorbed on the SnO_2–SnO during H_2S gas exposure, activating the H_2S reaction and leading in a reduction in resistance,

$$H_2S + 3O_{(ads)} \rightarrow SO_2 + H_2O + 3e^-.$$

The excited electrons were transferred from the conduction band of SnO_2–SnO to PGaN. The PGaN as an electrons acceptor suppressed charge recombination and resulted in more charge carriers to form reactive species. The sprayed SnO_2–SnO composites and the PGaN substrate formed together the continuous conductive pathways between the Ag electrodes. Meanwhile, the excellent transfer capability of PGaN contributed to the heightened electron transfer. The porous structure of GaN was more conducive to gas diffusion, compared with the Al_2O_3 substrate, which contributed plentiful adsorption of H_2S molecules. Therefore, the SnO_2–SnO/PGaN sensor exhibited better performance than the SnO_2–SnO/Al_2O_3 sensor.

The above is mainly the analysis of the sensor chemisorption–desorption model, while in most situations, physical adsorption–desorption has little effect on gas sensing performance and rarely discussed further, which only interferes with the directional movement of the surface carrier, leading to a slight increase in resistance.

4. Conclusion

In summary, an FSS/PGaN heterojunction was fabricated and the properties of the sensor based on the heterojunction have been investigated in-depth for the detection of H_2S. At the concentration of 50 ppm H_2S, the sensor exhibited excellent sensitivity, a fast response time of 65 s and a release time of 27 s at 150 °C. Compared with SnO_2–SnO/Al_2O_3 sensor, SnO_2–SnO/PGaN sensor showed the optimum temperature as low as 150 °C. Meanwhile, SnO_2–SnO/PGaN-based gas sensor showed enhanced H_2S sensing performance that could be attributed to the structure of PGaN itself and the heterojunction between SnO_2–SnO and PGaN. The study presented that, in addition to constructing sensitive p–n junction semiconductor materials, optimizing the substrate of sensitive materials is also a considerable manner to construct gas sensors with excellent sensing performance.

Acknowledgements

Project supported by the Natural Science Research Start-up Foundation of Recruiting Talents of Nanjing University of Posts and Telecommunications (Grant Nos. XK1060921115 and XK1060921002), Young Scientists Fund of the National Natural Science Foundation of China (Grant No. 62204125), the National Key R&D Program of China (Grant No. 2022YFB3605404), and the Natural Science Foundation of Guangdong Province, China (Grant No. 2019A1515010790).

References

[1] Pandey S K, Kim K H and Tang K T 2012 *TrAC Trends Anal. Chem.* **32** 87
[2] Chen H, Rim Y S, Wang I C, Li C, Zhu B, Sun M, Goorsky M S, He X and Yang Y 2017 *ACS Nano.* **11** 4710

[3] Srivastava S K, Magudapathy P, Gangopadhyay P, Amirthapandian S, Bera S and Das A 2019 *Thin Solid Films* **681** 86
[4] Kulkarni M R, John R A, Tiwari N, Nirmal A, Ng S E, Nguyen A C and Mathews N 2019 *Small* **15** 1901457
[5] Erme K and Jõgi I 2019 *Environ. Sci. Technol.* **53** 5266
[6] Bachhav M, Pawar G, Vurpillot F, Danoix R, Danoix F, Hannoyer B, Dong Y and Marquis E 2019 *J. Phys. Chem. C* **123** 1313
[7] Tiwari N, Nirmal A, Kulkarni M R, John R A and Mathews N 2020 *Inorg. Chem. Front.* **7** 1822
[8] Prati E, Michielis M D, Belli M, Cocco S, Fanciulli M, Patil D K, Ruoff M, Kern D P, Wharam D A, Verduijn J, Tettamanzi G C, Rogge S, Roche B, Wacquez R, Jehl X, Vinet M and Sanquer M 2012 *Nanotechnology* **23** 215204
[9] Cho S Y, Yoo H W, Kim J Y, Jung W B, Jin M L, Kim J S, Jeon H J and Jung H T 2016 *Nano Lett.* **16** 4508
[10] Youn Y, Lee M, Kim D, Jeong J K, Kang Y and Han S 2019 *Chem. Mater.* **31** 5475
[11] Boyal E, Baran V, Asar T, Özçelik S and Kasap M 2017 *J. Alloys Compd.* **692** 119e123
[12] Ma N, Suematsu K, Yuasa M, Kida T and Shimanoe K 2015 *ACS Appl. Mater. Interfaces* **7** 5863
[13] Motsoeneng R G, Kortidis I, Ray S S and Motaung D E 2019 *ACS Omega* **4** 3696
[14] Shanmugasundaram A, Basak P, Satyanarayan L and Manoram S V 2013 *Sens. Actuators B* **185** 265
[15] Song F, Su H L, Chen J J, Moon W J, Lau W M and Zhang D 2012 *J. Mater. Chem.* **22** 1121
[16] Wang Y, Liu C Y, Wang Z, Song Z W, Han N and Chen Y F 2019 *Sens. Actuators B* **278** 28
[17] Suman P H, Felix A A, Tuller H L, Varela J A and Orlandi M O 2015 *Sens. Actuators B* **208** 122
[18] Ozdemir S and Gole J L 2010 *Sens. Actuators B* **151** 274
[19] Dheyab A B, Alwan A M and Zayer M Q 2019 *Plasmonics* **14** 501
[20] Bilenko D I, Belobrovaja O Y, Coldobanova O Y, Jarkova E A, Khasina E I, Polyanskaya V P, Melnikova T E, Mysenko I B, Smirnov V V and Filippova G O 2000 *Sens. Actuators A* **79** 147
[21] Baratto C, Comini E, Faglia G, Sberveglieri G, Francia G D, Filippo F D, Ferrara V L, Quercia L and Lancellotti L 2000 *Sens. Actuators B* **65** 257
[22] Pancheri L, Oton C J, Gaburro Z and Pavesi L 2003 *Sens. Actuators B* **89** 237
[23] Xu K C, Lu Y Y and Takei K 2019 *Adv. Mater. Technol.* **4** 1800628
[24] Xu K C, Lu Y Y, Honda S, Arie T, Akita S and Takei K 2019 *J. Mater. Chem. C* **7** 9609
[25] Zhang M X, Zhao C H, Gong H M, Niu G Q and Wang F 2019 *ACS Appl. Mater. Interfaces* **11** 33124
[26] Zhang M R, Jiang Q M, Wang Z G, Zhang S H, Hou F and Pan G B 2017 *Sens. Actuators B* **253** 652
[27] Zhang M R, Hou F, Wang Z G, Zhang S H and Pan G B 2017 *Appl. Surf. Sci.* **410** 332
[28] Zhang M R, Qin S J, Peng H D and Pan G B 2016 *Mater. Lett.* **182** 363
[29] Zhong A H, Sasaki T and Hane K 2014 *Sens. Actuators A* **209** 52
[30] Luo X J, Zheng X J, Wang D, Zhang Y, Cheng H B, Wang X Y, Zhuang H J and Lou Y L 2014 *Sens. Actuators B* **202** 1010
[31] Abdullah Q N, Yam F K, Hassan J J, Chin C W, Hassan Z and Bououdina M 2013 *Int. J. Hydrogen Energy* **38** 14085
[32] Wang C, Huang H, Zhang M R, Song W X, Zhang L, Xi R, Wang L J and Pan G B 2019 *Nanoscale Adv.* **1** 1232
[33] Wang C, Wang L J, Zhang L, Xi R, Huang H, Zhang S H and Pan G B 2019 *J. Alloys Compd.* **790** 363
[34] Wang C, Zhang M R, Song W X, Peng H D, Huang H, Wang Z G, Xi R and Pan G B 2018 *Chem. Phys. Lett.* **710** 54
[35] Shankar P and Rayappan J B B 2017 *J. Mater. Chem. C* **5** 10869
[36] Wang Y, Qu F, Liu J, Wang Y, Zhou J and Ruan S 2015 *Sens. Actuators B* **209** 515
[37] Kheel H, Sun G J, Lee J K, Lee S, Dwivedi R P and Lee C 2016 *Ceram. Int.* **42** 18597
[38] Jiang P, Zhang H, Chen C, Liang J, Luo Y, Zhang M and Cai M 2017 *Cryst. Eng. Comm.* **19** 5742
[39] Song Z, Wei Z, Wang B, Luo Z, Xu S, Zhang W, Yu H, Li M, Huang Z, Zang J, Yi F and Liu H 2016 *Chem. Mater.* **28** 1205
[40] Guo W, Mei L, Wen J and Ma J 2016 *RSC Adv.* **6** 15048
[41] Hong P P, Manh H C, Toan N V, Duy N V, Duc H N and Hieu N V 2020 *Sens. Actuators A* **303** 111722
[42] Ji H, Zeng W and Li Y 2019 *Nanoscale* **11** 22664
[43] Wang X, Wang Y, Tian F, Liang H, Wang K, Zhao X, Lu Z, Jiang K, Yang L and Lou X 2015 *J. Phys. Chem. C* **119** 15963
[44] Yousefi S M, Rahbarpour S and Ghafoorifard H 2019 *Mater. Chem. Phys.* **227** 148
[45] Selvaraj K, Kumar S and Lakshmanan R 2014 *Ain. Shams Eng. J.* **5** 885
[46] Yang S, Wang Z, Zou Y, Luo X, Pan X, Zhang X, Hu Y, Chen K, Huang Z, Wang S, Zhang K and Gu H 2017 *Sens. Actuators B* **248** 160
[47] Liu Y, Jiao Y, Zhang Z L, Qu F Y, Umar A and Wu X 2014 *ACS Appl. Mater. Interfaces* **6** 2174
[48] Zappa D, Galstyan V, Kaur N, Arachchige H M M, Sisman O and Comini E 2018 *Anal. Chim. Acta* **1039** 1